Time-Domain Electromagnetic Modeling and Simulation of a Nonlinear Electro-Optical Mixer

Arif Can Gungor(✉), Hande Ibili, Jasmin Smajic, and Juerg Leuthold

Institute of Electromagnetic Fields (IEF), ETH Zurich, 8092 Zurich, Switzerland
arifg@ethz.ch

Abstract. A full-wave electromagnetic solver coupled with a Poisson's solver based on time-domain finite element method (TD-FEM) is developed. This solver aims to simulate the side-band frequency generation on optical signal due to the imposed radio frequency (RF) signal through a nonlinear material. The optical signal propagating within an optical waveguide is simulated in time-domain by solving the electromagnetic wave equation, whereas Poisson's equation is numerically solved to compute the strength of the slowly-varying RF signal. The applied RF signal changes the permittivity of the nonlinear material BTO, and this changing permittivity affects the transient wave behavior of the light. As opposed to the available frequency-domain Maxwell solvers, this proposed time-domain solver is capable of simulating the nonlinear effects introduced by an electro-optical material, and implemented for the modeling of an application where RF signal is mixed into the optical frequencies. As a result of the simulations, nonlinear dielectric constant of electro-optical material is computed, and resulting side-band frequency generation is observed in the spectrum of the time-domain output signal.

1 Introduction

New generation mobile network systems offer faster communication speeds and extensive data transfer rates. New 5G and 6G applications utilize higher frequency bands to satisfy the demand in broader bandwidths and high data transfer rates, and photonic and plasmonic communication systems proved to be vital in this pursuit to replace highly lossy traditional electronic counterparts. In [1–5] authors have successfully demonstrated plasmonic modulation and photodetection reaching up to 500 GHz. Furthermore, a transparent optical-subTHz-optical link with single line rate of 240 Gbit/s over 115 m at subTHz frequencies over 200 GHz is reported [5]. The permanent progress in high frequency communication systems and continuous increase in data transfer rates rely on conversion of electronic and optical signals to each other [6], and ultra-fast, energy-efficient electro-optical switches. Recently, electro-optic modulation schemes via quantum effects [7], 2D materials [8], resonant structures [9], or plasmonic effects [10] have been demonstrated. To avoid the speed limitations that can be introduced by some of these methods, electro-optic devices with plasmonics that enhances the nonlinear effects via light confinement into sub-diffraction limits are reported [11]. Including plasmonics,

M. van Beurden et al. (Eds.): SCEE 2022, MI 43, pp. 86–93, 2024.
https://doi.org/10.1007/978-3-031-54517-7_10

one common way of mixing optical and electrical signals is through phase modulation of an optical signal by an RF signal that produces a series of side-band frequencies in the optical domain by utilizing nonlinear materials [12]. Therefore, advanced nonlinear electro-optical devices offer solutions for the next generation high speed communication systems. The performance of these devices are strongly dependent on the electro-optic coefficients of these nonlinear materials [13]. Moreover, the physical properties of the waveguides and light confinement are affecting the device operation as well [14]. Consequently, this article focuses on time-domain modeling of phase modulation of an optical signal and the mentioned nonlinear electro-optical effect. The objective of this article is to present a nonlinear material integrated optical waveguide in order to observe and model the mixing of the RF frequencies to the optical frequencies.

This article is organized as follows. Section 2 presents the optical waveguide and the material nonlinearity, as well as theoretical backgrounds for the computation. Section 3 discusses the results and Sect. 4 concludes the paper with remarks and future work description.

2 Physical Model and Theory

Considered problem requires electromagnetic analysis of an optical waveguide structure that has a nonlinear material insertion. The defined scheme is depicted in Fig. 1a, which consists of a 2-D optical waveguide, and in its middle section, a nonlinear material, Barium Titanate (BTO), is inserted as a phase modulator. Electric permittivity ε_{rBTO} of BTO depends on the electric field $|E_{local}|$ it encounters, and can provide Pockels coefficients as high as 1600 pm/V [15,16]. Assuming single crystal BTO, the relation between the permittivity of BTO and the electric field is given as follows [16]:

$$\varepsilon_{rBTO}(|E_{local}|) = \frac{\varepsilon_0}{\left(1 + k\varepsilon_0^3 |E_{local}|^2\right)^{1/3}}, \tag{1}$$

where $\varepsilon_0 = 1000$ is the typical zero-field permittivity for BTO, and $k = 3\beta\varepsilon_0^3 = 10^{-8} m^2 V^{-2}$ is a constant that includes the nonlinear Johnson's parameter β.

The core material of the waveguide has 400 nm width and is assumed to be Silicon (with $\varepsilon_{rSi} = 12.04$). Whereas the cladding is 2 μm wide on each side of the waveguide and is taken as Silicondioxide ($\varepsilon_{rSiO_2} = 2.07$). The electro-optical (EO) modulator section with BTO insertion is chosen such that the effective permittivity of that section varies as $\varepsilon_r = 0.9\varepsilon_{rSi} + 0.1\varepsilon_{rBTO}$, since the fabricated 3-D devices have dominant contributions from the core material in addition to the deposited BTO. In other words, the EO section consists of a layer of BTO on the Silicon waveguide which leads to consideration of an effective electric permittivity that is combination of electric permittivities of Silicon and BTO.

The electromagnetic solver is developed using electromagnetic wave equation in time domain as in (2). The boundary conditions are perfect electric conductor (PEC) boundary condition on the top and the bottom sides of the structure ($\mathbf{n} \times \mathbf{E} = 0$, where $\mathbf{n}$ is unit vector pointing outwards direction), and the port boundary condition (3) is used for both the input and the output waveports (without excitation at the output, $\mathbf{E_0} = 0$). On the other hand, the field distribution due to the applied RF signal is computed by

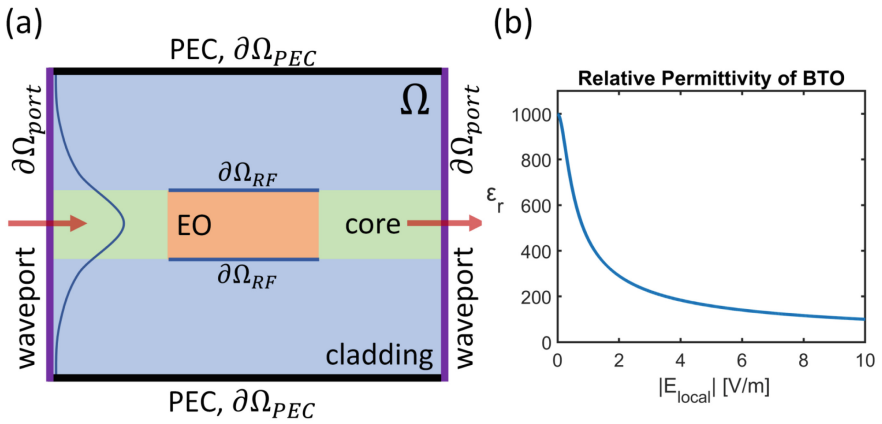

Fig. 1. Figure illustrating the nonlinear electro-optical signal mixer. (a): 2-D optical waveguide is depicted. The input waveport is on the left, whereas the output is on the right. The core section has also an electro-optical (EO) phase modulator (the middle part) in the middle to provide the nonlinearity. (b): Relative permittivity ε_r vs. $|E_{local}|$ is shown for the pure nonlinear material. The RF signal is directly applied on the contacts ($\partial\Omega_{RF}$) near the nonlinear material whereas the light excitation is provided from the waveport ($\partial\Omega_{port}$) on the left, and it is absorbed from the right.

the Poisson's equation as in (4). The RF signals are applied as Dirichlet conditions on the boundaries of the electro-optical (EO) material as in (5) and PEC boundary conditions are implemented for the computation domain boundaries for the RF field analysis ($\varphi = 0$ on outer boundaries).

The computed potential distribution φ is used to obtain the RF field $\mathbf{E}_{RF} = -\nabla\varphi$ and $|E_{local}| = |\mathbf{E}_{RF}|$ since the RF field (in the order of V/m) is much higher than the optical field (in the order of $\mu V/m$). Then, $|E_{local}|$ is used to compute the electric permittivity of BTO and the effective electric permittivity of the phase modulator sections based on (1).

For this coupled analysis to be accurate, the main assumptions are that the wavelength of the RF signal (in the order of millimeters) is very large compared to the computation domain (in the order of micrometers), and RF signal also varies very slowly compared to the time domain optical signal. Therefore, it is safe to solve only Poisson's equation for the RF field and resultant nonlinear contribution. Furthermore, the given waveguide is single-moded and the fundamental mode operation only requires z-component of the electric field for the light propagation. Consequently, Eq. (2) can be further reduced to a scalar equation which is be very convenient for the numerical analysis.

$$\nabla \times \left(\frac{1}{\mu_r}\nabla \times \mathbf{E}\right) + \mu_0\sigma\frac{\partial \mathbf{E}}{\partial t} + \mu_0\varepsilon_0\varepsilon_r\frac{\partial^2 \mathbf{E}}{\partial t^2} = 0 \; in \; \Omega \tag{2}$$

$$\mathbf{n}\times\left(\frac{1}{\mu_r}\nabla\times\mathbf{E}\right)+\frac{\mu_0}{Z_{port}}\mathbf{n}\times\left(\mathbf{n}\times\frac{\partial\mathbf{E}}{\partial t}\right) = \frac{-2\mu_0}{Z_{port}}\mathbf{n}\times\left(\mathbf{n}\times\frac{\partial\mathbf{E_0}}{\partial t}\right) \quad over\ \partial\Omega_{port} \tag{3}$$

$$\nabla(\varepsilon\nabla\varphi)=0\ in\ \Omega \tag{4}$$

$$\varphi=\varphi_{RF}\ over\ \partial\Omega_{RF} \tag{5}$$

$$\frac{\partial\mathbf{E}}{\partial t}\approx\frac{\mathbf{E}_t-\mathbf{E}_{t-1}}{\Delta t} \tag{6}$$

The introduced equations are discretized using Finite Element Method (FEM) and using first order linear shape functions by adopting the formulation in [17] and [18]. This discretization resulted around 14000 triangular elements for the complete geometry. The time discretization is done by Backward Difference Formula (BDF) as in (6) that ensures the stability of the wave equation [18]. Furthermore, the coupling of the wave equation (2) and the Poisson's equation is done through the effective permittivity of the EO material which directly effects the wave propagation. The time-domain approach requires very small time steps in the order of femtoseconds (0.1–1 fs) for the full wave simulation of the propagating light, whereas the RF field is changing very slowly and hence solving the static Poisson's equation at every time step is sufficient. In other words, the static Poisson's equation is solved at every time step to compute the RF field and the instantaneous effective permittivity before solving the wave equation in the respective time step. One complete simulation with sufficient number of periods of the optical signal requires around 200 MB memory, and it takes around 0.3 s CPU time for the computation of a single time step on an Intel i7-7500 CPU. A snapshot of the electric field (E_z) with the propagating fundamental mode is shown in Fig. 2 where the scattering due to nonlinear material is visible.

3 Results

The influence of the 'slowly varying' RF field directly reveals itself on the propagating light due to nonlinear electric permittivity of the EO section. From the input port, optical wave with wavelength of 1550 nm is excited with the spatial shape of the fundamental mode of the single-moded waveguide. Fast Fourier Transform (FFT) of the input signal, (the blue curve in Fig. 3b) also proves the excitation initially has purely one wavelength. After propagating through the waveguide and going through the nonlinear EO material in the presence of an RF excitation of 500 GHz, light reaches the output waveport, where its FFT is again computed. Figure 3b clearly shows that at the output, in addition to the excitation signal, other frequencies emerge. These frequencies occur at $f_{out}=f_0\pm mf_{RF}$, where f_0 denotes the original optical carrier frequency, f_{RF} is the RF frequencies applied to EO section and $m=\pm1,\pm2,...$ is an integer. With the applied RF field in this simulated case, ε_{rBTO} changes between around 25 and 100, which in return provides the mixing of RF signal into the optical carrier signal.

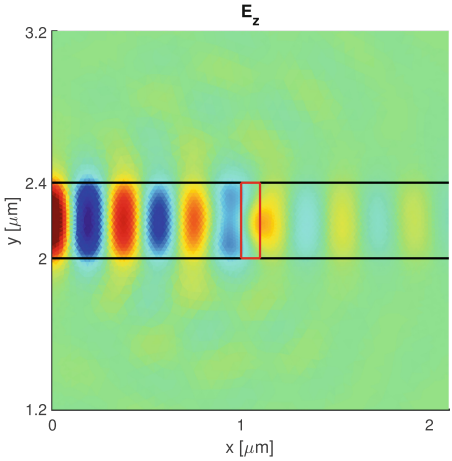

Fig. 2. Snapshot of the normalized field due to propagating light in the given waveguide with the nonlinear insertion. Here the plot depicts the z-component of the propagating electric due to light, and the applied in-plane RF field is not shown. Light enters into the computation domain from the left boundary, where the fundamental mode excitation (having only z-component) is applied, and travels within the Si core between the black lines; and absorbed at the output port on the right. The box, with 100 nm length (in x dimension), indicates where BTO is inserted. Scattering of the light due to discontinuity of permittivity can be seen.

Furthermore, amplitude of the applied RF signal have an effect on how efficient the signal mixing takes place. This also reveals itself as changing side-band ratios in the spectrum of the output signal. In other words, the emerging side-band frequencies have different peaks and different ratios with respect to the central optical frequency f_0. This can be observed in Fig. 4, as the higher RF field amplitude results higher sideband peaks when the spectrum are all normalized with respect to the central peak f_0. Also in Fig. 5, the side-band ratios for the first three side-bands are given with respect to varying RF field amplitude. Since the permittivity dependence of the BTO is nonlinear with respect to E_{local}, the side-band ratios also change nonlinearly and they saturate, which makes the design of electro-optical signal mixers more challenging and interesting.

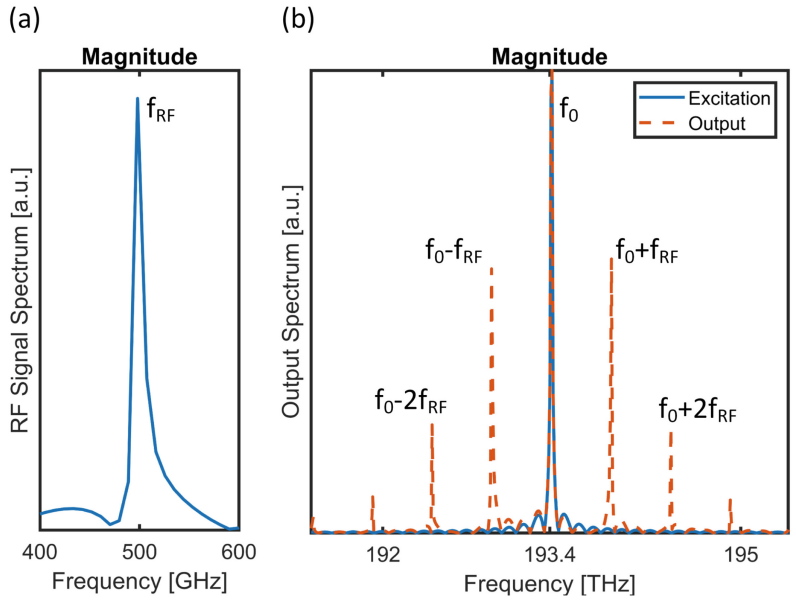

Fig. 3. Figure showing the spectrum of the signals indicating the signal mixing at the output. (a): Spectrum of the RF signal, single peak at 500 GHz. (b): Normalized spectrum of the optical signals: excitation signal, and the signal at the output port. The spectrum of the output optical signal shows that side-band frequencies are generated at $f_{out} = f_0 \pm m f_{RF}$.

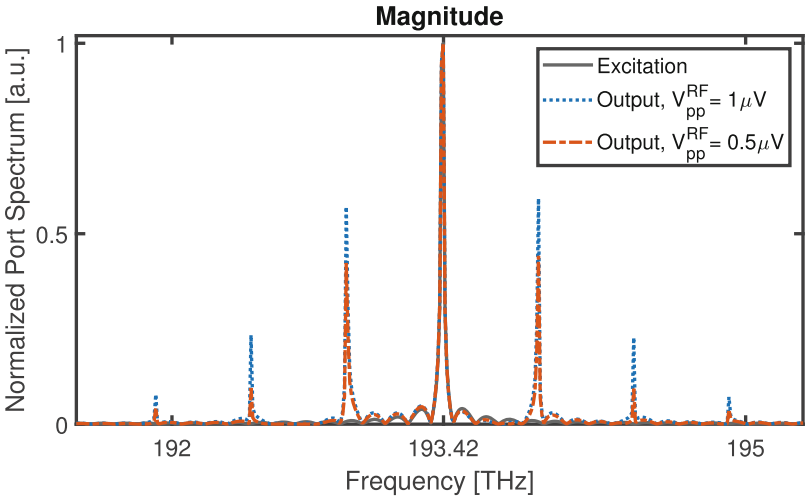

Fig. 4. Normalized (with respect to corresponding f_0 peak) spectrum of the mixed signals when different RF amplitudes are applied. The two curves depict the spectrum when the peak-to-peak potential through the EO section is 0.5 μV and 1.0 μV. As expected, high RF field results side-bands with higher amplitude, but the effect is nonlinear due to material's field dependent electric permittivity.

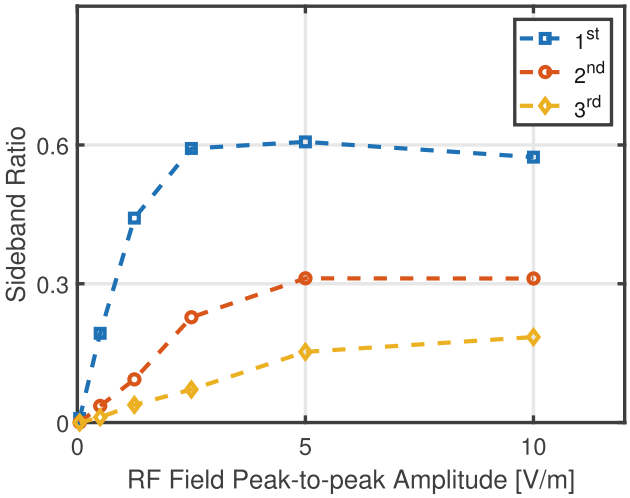

Fig. 5. 1st, 2nd and 3rd sideband ratios with respect to changing RF field peak-to-peak amplitude. The ratios are calculated from the amplitudes of the respective peak and the central peak at the output.

4 Conclusion

Thanks to the developed solver, nonlinear EO materials can be considered accurately and the effects can be observed directly. Additionally, Pockels coefficient of nonlinear materials for a given structure can be determined and verified using this method starting from the basic material properties. Therefore, this work opens up new perspective to improve the design of electro-optical high-speed devices by enabling simulation of more complicated modulator structures, side-band frequency generation and signal mixing by nonlinear materials. Using the developed solver, it is possible to optimize the device structures and dimensions to make use of the nonlinear effects and to efficiently obtain signal mixing while maintaining high signal-to-noise ratios. Moreover, this approach could offer additional physics coupling such as charge transport in the active material due to RF signal or DC bias [19,20], and nonlinear effects of the moving charges can also be inserted. Besides, explicit discontinous Galerkin time-domain methods can easily be applied for the Maxwell's equations to eliminate the computational costs introduced due to the costly matrix inversions and dynamic matrix assembly operations at every time step that result from the nonlinear material properties. We also plan to extend our studies by performing a full stability analysis of the coupled system for various time discretization methods.

References

1. Haffner, C., et al.: All-plasmonic Mach-Zehnder modulator enabling optical high-speed communication at the microscale. Nat. Photonics **9**, 525–528 (2015)
2. Burla, M., et al.: 500 GHz plasmonic Mach-Zehnder modulator enabling sub-THz microwave photonics. APL Photonics **4**, 056106 (2019)
3. Salamin, Y., et al.: 300 GHz plasmonic mixer. In: IEEE 2019 International Topical Meeting on Microwave Photonics (MWP), pp. 1-4 (2019)
4. Koepfli, S., et al.: High-speed graphene photodetection: 300 GHz is not the limit. In: 2021 Conference on Lasers and Electro-Optics Europe & European Quantum Electronics Conference (2021)
5. Horst, Y., et al.: transparent Optical-THz-optical link at 240/192 Gbit/s over 5/115 m enabled by plasmonics. J. Lightwave Technol. (2022)
6. Hu, Y., et al.: On-chip electro-optic frequency shifters and beam splitters. Nature **599**, 587–593 (2021)
7. Segev, A., Sa'ar, A., Oiknine-Schlesinger, J., Ehrenfreund, E.: Quantum interference versus Stark intersubband electro-optical modulation in asymmetrical quantum wells. Superlattices Microstruct. **19**, 47–57 (1996)
8. Sun, Z., Martinez, A., Wang, F.: Optical modulators with 2D layered materials. Nat. Photonics **10**, 227–238 (2016)
9. Timurdogan, E., Sorace-Agaskar, C.M., Sun, J., Shah Hosseini, E., Biberman, A., Watts, M.R.: An ultralow power athermal silicon modulator. Nat. Commun. **5**, 1–11 (2014)
10. Davis, T.J., Gómez, D.E., Roberts, A.: Plasmonic circuits for manipulating optical information. Nanophotonics **6**, 543–559 (2017)
11. Lee, H., et al.: Nanoscale conducting oxide PlasMOStor. Nano Lett. **14**, 6463–6468 (2022)
12. Abel, S., et al.: Large Pockels effect in micro-and nanostructured barium titanate integrated on silicon. Nat. Mater. **18**, 42–47 (2019)
13. Boyd, R. W.: Nonlinear Optics. Academic Press (2020)
14. Heni, W., et al.: Nonlinearities of organic electro-optic materials in nanoscale slots and implications for the optimum modulator design. Opt. Express **25**, 2627–2653 (2017)
15. Li, M., Tang, H.X.: Strong pockels materials. Nat. Mater. **18**, 9–11 (2019)
16. Padurariu, L., Curecheriu, L., Buscaglia, V., Mitoseriu, L.: Field-dependent permittivity in nanostructured BaTiO3 ceramics: modeling and experimental verification. Phys. Rev. B **85**, 224111 (2012)
17. Gungor, A.C., Celuch, M., Smajic, J., Olszewska-Placha, M., Leuthold, J.: Electromagnetic and semiconductor modeling of scanning microwave microscopy setups. IEEE J. Multiscale Multiphys. Comput. Tech. **5**, 209–216 (2020)
18. Jin, J.M.: The Finite Element Method in Electromagnetics. Wiley, Hoboken (2015)
19. Gungor, A.C., Ehrengruber, T., Smajic, J., Leuthold, J.: Coupled electromagnetic and hydrodynamic modeling for semiconductors Using DGTD. IEEE Trans. Magn. **57**, 1–5 (2021)
20. Gungor, A.C., Doderer, M., Ibili, H., Smajic, J., Leuthold, J.: Coupled electromagnetic and hydrodynamic semiconductor modeling for Terahertz generation. IEEE Trans. Magn. (2022)